Optical investigation of gas-phase KCl/KOH sulfation in post flame conditions

Weng, Wubin; Chen, Shuang; Wu, Hao; Glarborg, Peter; Li, Zhongshan

Published in:
Fuel

DOI:
10.1016/j.fuel.2018.03.095

2018

Document Version:
Publisher's PDF, also known as Version of record

Fuel 224 (2018) 461–468

Contents lists available at ScienceDirect

Fuel

journal homepage: www.elsevier.com/locate/fuel

Full Length Article

Optical investigation of gas-phase KCl/KOH sulfation in post flame conditions

Wubin Weng[a], Shuang Chen[a,b], Hao Wu[c], Peter Glarborg[c], Zhongshan Li[a,*]

[a] Division of Combustion Physics, Lund University, P.O. Box 118, SE221 00 Lund, Sweden
[b] China Aerodynamics Research and Development Center, Mianyang, China
[c] Department of Chemical and Biochemical Engineering, Technical University of Denmark, DK-2800 Kgs. Lyngby, Denmark

ARTICLE INFO

Keywords:
Sulfation
Potassium hydroxide
Potassium chloride
Counter-flow
Aerosol

ABSTRACT

A counter-flow reactor setup was designed to investigate the gas-phase sulfation and homogeneous nucleation of potassium salts. Gaseous KOH and KCl were introduced into the post-flame zone of a laminar flat flame. The hot flame products mixed in the counter-flow with cold N_2, with or without addition of SO_2. The aerosols formed in the flow were detected through Mie scattering of a 355 nm laser beam. The temperature distribution of the flow was measured by molecular Rayleigh scattering thermometry. From the temperature where nucleation occurred, it was possible to identify the aerosols formed. Depending on the potassium speciation in the inlet and the presence of SO_2, they consisted of K_2SO_4, KCl, or K_2CO_3, respectively. The experiments showed that KOH was sulphated more readily than KCl, resulting in larger quantities of aerosols. The sulfation process in the counter-flow setup was simulated using a chemical kinetic model including a detailed subset for the Cl/S/K chemistry. Similar to the experimental results, much more potassium sulfate was predicted when seeding KOH compared to seeding KCl. For both KOH and KCl, sulfation was predicted to occur primarily through the reactions among atomic K, O_2 and SO_2, forming $KHSO_4$ and K_2SO_4. The higher propensity for sulfation of KOH compared to KCl was mostly attributed to the lower thermal stability of KOH, facilitating formation of atomic K. According to the model, sulfation also happened through SO_3, especially for KCl ($KCl \rightarrow KSO_3Cl \rightarrow K_2SO_4$).

1. Introduction

Biomass, including energy crops [1], agricultural products [2] and industrial biomass waste [3], is considered as a sustainable and carbon neutral energy source. It is commonly combusted in boilers to provide heat and/or power. However, biomass such as agricultural residues may contain relatively high concentrations of potassium, chlorine and sulfur. During combustion, these elements lead to the formation of potassium chloride (KCl), potassium hydroxide (KOH), hydrogen chloride (HCl) and sulfur dioxide (SO_2), causing problems of slagging and fouling, corrosion, and emissions of harmful gases and aerosols [2]. The presence of KCl in the flue gas may cause severe ash deposition and corrosion on the super-heater tubes [4]. Sulfation of KCl to K_2SO_4 by reaction with sulfur-containing additives [5–7] has been suggested as a method to mitigate deposition and corrosion processes, since K_2SO_4 is less corrosive and has a higher melting point than KCl.

Sulfation can occur via homogenous reactions between gas-phase KCl/KOH and sulfur oxides, i.e. SO_2 and SO_3. There are several studies on the sulfation of gaseous KCl [5,7–16]. A detailed chemical mechanism was proposed by Glarborg and Marshall [10], involving the following reactions:

$$KCl + SO_3(+M) = KSO_3Cl(+M) \quad (R1)$$

$$KOH + SO_3(+M) = KHSO_4(+M) \quad (R2)$$

$$KSO_3Cl + H_2O = KHSO_4 + HCl \quad (R3)$$

$$KHSO_4 + KCl = K_2SO_4 + HCl \quad (R4)$$

$$KHSO_4 + KOH = K_2SO_4 + H_2O \quad (R5)$$

This mechanism was proven to be consistent with the experimental results of Iisa et al. [8]. The oxidation of SO_2 to SO_3 was considered to be the rate-limiting step. The importance of SO_3 has been supported by several experimental studies, e.g. [7,13].

More recently, Hindiyarti et al. [11] proposed a number of alternative sulfation routes to explain the observed sulfation rates at lower temperatures. One pathway involved the direct reaction between KOH and SO_2 to form $KHSO_3$, with oxidation of sulfite to sulfate as the rate-limiting step, instead of the oxidation of SO_2 to SO_3:

* Corresponding author.
E-mail address: zhongshan.li@forbrf.lth.se (Z. Li).

https://doi.org/10.1016/j.fuel.2018.03.095
Received 24 January 2018; Received in revised form 7 March 2018; Accepted 13 March 2018
Available online 20 March 2018

$$KOH + SO_2(+M) = KHSO_3(+M) \quad (R6)$$

$$KHSO_3 + O_2 = KHSO_4 + O \quad (R7)$$

Another route of K_2SO_4 formation can be initiated by the reaction of atomic K with SO_2, forming KOSO, which is then oxidized to $KOSO_3$ and further to $KHSO_4$. These suggested pathways have not been confirmed experimentally, even though they are consistent with results reported by Kassman et al. [13] and Ekvall et al. [15,16].

To evaluate the detailed reaction mechanism, Li et al. [14] studied the formation of K_2SO_4 from gas-phase KCl and SO_2 in a homogeneous high temperature environment produced by a laminar burner where neither wall-based reactions nor other heterogeneous reactions could contribute to the sulfation processes. The study supported the importance of the reaction sequence R1, R3 and R4 for the sulfation of KCl.

Previous efforts have mostly focused on the sulfation of KCl. However, in combustion of low-chlorine woody biomass KOH is typically formed in larger concentrations than KCl. Despite the importance, knowledge on sulfation of KOH is still limited. In the present work, sulfation of both KOH and KCl was studied in a specially designed counter-flow reactor. Gas-phase KOH and KCl were provided by feeding micro droplets of KCl/KOH water solutions to the hot flue gas from a premixed CH_4/air flame, having an equivalence ratio of 0.9 or 1.1. The combustion products including the gaseous potassium compounds then mixed with an opposed N_2 flow containing SO_2 to form a gas-phase counter-flow configuration. The temperature distribution was measured and the aerosols formed in the flow were detected. The results were interpreted in terms of an updated chemical kinetic model for Cl/S/K interactions to provide a better understanding of the sulfation process.

2. Experiment and simulation

2.1. Burners

A schematic of the counter-flow burner setup is shown in Fig. 1. A uniform laminar N_2 flow seeded with a known amount of SO_2 was supplied through a 60 mm diameter sintered-metal porous plug of a

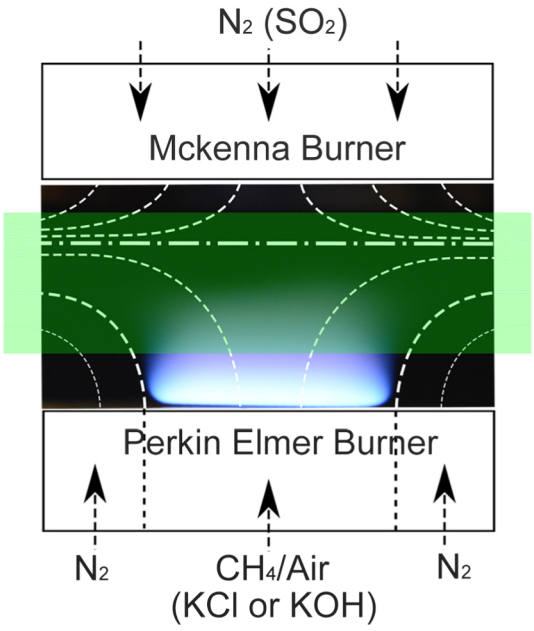

Fig. 1. Schematic of the counter-flow setup together with a photo of a typical flame adopted in the experiment. The white dash lines depict the flow field. The light green square indicates the region illuminated by the laser sheet. (For interpretation of the references to color in this figure legend, the reader is referred to the web version of this article.)

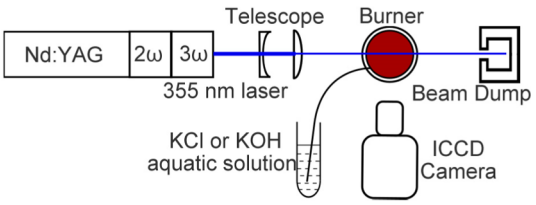

Fig. 2. Schematic of the laser measurement system.

McKenna burner. The outlet flow speed was 10 cm s^{-1} and the temperature was 298 K. The concentration of SO_2 in the flow was set to 0 ppm, 245 ppm or 980 ppm, respectively.

A uniform laminar hot flue gas was generated on a Perkin Elmer burner, modified to allow for seeding of water solutions [17]. A chamber connected to an upper honeycomb matrix with a diameter of 23 mm was used to mix methane and air for the burner. In the present study, a premixed CH_4/air flow with an unburned gas speed of 15 cm s^{-1} was used to generate a flat laminar flame at an equivalence ratio of either 0.9 or 1.1 above the burner. An aqueous solution containing potassium chloride or potassium hydroxide was seeded homogeneously into the flame by a nebulizer as shown in Fig. 2. The salt concentration of the aqueous solution was 0.5 mol l^{-1}, and the concentration of the gas-phase potassium chloride or potassium hydroxide in the hot flue gas was calculated to be around 215 ppm based on the consumption rate. A N_2 co-flow at room temperature was used to shield the flame from the ambient air with an exit flow speed of 15 cm s^{-1}. The distance between the Perkin Elmer burner and the McKenna burner was 20 mm. A stable counter-flow was formed between the N_2 flow from the McKenna burner and the hot flue gas from the Perkin Elmer burner. The reactions between SO_2 and KCl/KOH occurred in the mixing zone.

2.2. Laser measurement system

When the flue gas containing KCl or KOH mixed with the cold N_2 (SO_2) flow, the temperature decreased to ~1000 K and aerosols were formed. The aerosols were detected from the Mie scattering when illuminated by a 355 nm laser beam from the third harmonic of a Nd:YAG laser (Brilliant B, Quantel) operated at 10 Hz with a pulse energy of 50 mJ, formed into a laser sheet using a telescope lens system. The laser sheet passed through the counter-flow region vertically as depicted in Fig. 1. The signal of the Mie scattering from the aerosols was detected by an intensified CCD camera (ICCD, PI-MAX II, Princeton Instruments). No laser breakdown was observed from illumination of the aerosols.

Using the same system, the temperature distribution of the counter-flow was measured through Rayleigh scattering thermometry based on the following equation [18]:

$$T_{flow\ gas} = T_{air}(I_{air}/I_{flow\ gas})(\sigma_{flow\ gas}/\sigma_{air}) \quad (1)$$

where $T_{flow\ gas}$ is the temperature of the counter-flow, T_{air} is the temperature of the reference gas, i.e., the ambient air, which had a temperature of 298 K, $I_{flow\ gas}$ and I_{air} are the Rayleigh scattering signals of the counter-flow gas and the room temperature air, which can be obtained by the laser setup shown in Fig. 2, and $\sigma_{flow\ gas}$ and σ_{air} are the molecular Rayleigh scattering cross sections of counter-flow gas and air. For the Rayleigh scattering cross sections, the same value was used during the temperature calculation. The uncertainty of the obtained temperature caused by the cross section difference between air and the counter flow gas was estimated to be less than 25 K for the temperature at 700 K.

2.3. Numerical approach

The sulfation reaction in the present setup was simulated using the

counter-flow application code in CHEMKIN [19]. The composition of the hot flue gas was obtained based on the one-dimensional modeling of the premixed CH_4/air flame at an equivalence ratio (ϕ) of 0.9 or 1.1. The flue gas in the post flame, 3 mm from the flame front, was used as the inlet gas of the counter-flow model, which had a temperature of 2060 K (ϕ = 0.9) or 2118 K (ϕ = 1.1). Hence, the inlet speed setting was 103 cm s^{-1} (ϕ = 0.9) or 107 cm s^{-1} (ϕ = 1.1). The concentration of the gas-phase KCl or KOH in the flue gas was set to 215 ppm. The cool N_2 flow had an inlet temperature and flow speed of 298 K and 10 cm s^{-1}, respectively. If added, the concentration of SO_2 in the N_2 flow was either 245 ppm or 980 ppm. The distance between the two flow inlets was 20 mm.

A potassium sulfation mechanism was adopted for the simulations, based on previous work [10,11,14]. The reaction subsets and thermodynamic properties for H_2 oxidation [20], sulfur chemistry [21], and chlorine chemistry [22] were updated following recent developments. In the present work, the alkali chemistry was revised, with a particular emphasis on the sulfation pathways for KOH and KCl. The full mechanism is available as Supplementary Material.

As discussed in the Introduction, Glarborg and Marshall [10] proposed a mechanism for gas-phase sulfation of KCl. The rate limiting step was the oxidation of SO_2 to SO_3, followed by the fast sequence KCl + SO_3(+M) = KSO_3Cl(+M) (R1), KSO_3Cl + H_2O = $KHSO_4$ + HCl (R3), $KHSO_4$ + KCl = K_2SO_4 + HCl (R4). Modeling studies indicate that this mechanism can explain sulfation rates for KCl obtained in laboratory flow reactors, entrained-flow reactors and premixed flames [10,11,14]. However, the generation of O/H radicals is limited at low temperatures, and under these conditions the oxidation of SO_2 to SO_3 is too slow to explain observed the sulfation rate.

In an exploratory study, Hindiyarti et al. [11] proposed a number of alternative sulfation pathways that did not involve SO_3 as an intermediate. Below we re-evaluate these pathways, since they may be important for the sulfation of KOH. Hindiyarti et al. often employed upper limit rate constants for the involved reactions and we have re-evaluated some of these values. The sequence KOH + SO_2(+M) = $KHSO_3$(+M) (R6), $KHSO_3$ + O_2 = $KHSO_4$ + O (R7) was of particular interest since it did not involve any radicals as reactants and thereby could occur at lower temperatures. Hindiyarti et al. entered the rate limiting step R7 in the reverse direction, $KHSO_4$ + O = $KHSO_3$ + O_2 (R7b) and assumed the reaction to be fast. However, the step involves the breaking of an S=O double bond and we anticipate the reaction to be significantly slower, estimating k_{7b} by analogy to SO_3 + O.

Another proposed sequence involves $KOSO_2$, KO + SO_2(+M) = $KOSO_2$(+M) (R8), $KOSO_2$ + OH (+M) = $KHSO_4$ (+M) (R9). By analogy to K + SO_2 (+M), reaction R8 is presumably fast and the second step is expected to be rate limiting. We have updated our estimate of k_9 based on the observation that reactions of alkali species with radicals are not very fast and that the reaction is presumably at its low pressure limit.

Alternatively, $KHSO_4$ could be formed by the sequence K + O_2 (+M) = KO_2 (+M) (R10), KO_2 + SO_2 (+M) = $KOSO_3$(+M) (R11), $KOSO_3$ + H_2O = $KHSO_4$ + OH (R12). The thermodynamic properties for KO_2 and the rate constant for R10 were adopted from Sorvajärvi et al. [23]. The rate limiting step in this sequence is expected to be reaction R12. This reaction is now included in the mechanism in the reverse direction, $KHSO_4$ + OH = $KOSO_3$ + H_2O (R12b) with a rate constant assumed to be similar to that of $HOSO_2$ + OH = SO_3 + H_2O.

3. Results and discussion

A photo of the premixed flame at an equivalence ratio of 0.9 is presented in Fig. 3(a). Potassium chloride aqueous solution was seeded homogeneously into the flame as small droplets from the Perkin Elmer burner. The chemiluminescence of the excited K atom at a wavelength of 404 nm can be observed in the light bluish hot flue gas above the flat flame. As the flue gas approached chemical equilibrium and the temperature decreased above the height of ~12 mm, the chemiluminescence disappeared. The signal of the Rayleigh/Mie scattering in the region marked by the red dash lines in Fig. 3(a) was captured by the ICCD camera. The Rayleigh scattering signal of the counter-flow with pure water seeding is shown in Fig. 3(b). The scattering signal with KCl solution seeding is shown in Fig. 3(c). Comparing to the Rayleigh scattering signal shown in Fig. 3(b), the only difference in Fig. 3(c) is the appearance of a thin strong signal at the contact area between the hot flue gas and the cold nitrogen flow from the McKenna burner and the co-flow. The data at a given height of 6 mm is plotted in Fig. 3(d). The good agreement between the Rayleigh scattering signals of these two measurements indicates that the temperature distribution is not affected by the introduction of KCl.

The temperature distribution of the counter-flow was calculated based on Eq. (1). Fig. 4 compares the measured and predicted temperature profiles from the fuel-lean and the fuel-rich flame, respectively. The predicted temperature profile has been shifted by 0.3 mm compared to the measured values to compensate for minor non-idealities in the experiment. The figure also indicates the location of the stagnation plane for the two flames.

The strong signal from the Mie scattering of aerosols shown in Fig. 3(c) indicates that some gas-phase KCl underwent homogeneous nucleation in the low-temperature region. Combining the results of the Mie and Rayleigh scattering, it can be seen that aerosols of KCl in Fig. 3(c) are mainly formed in the region with a temperature between 700 K and 1000 K; this is discussed in more detail below.

The signal of the Mie scattering under different seeding conditions is presented in Fig. 5 for the lean flame (ϕ = 0.9). The signal was obtained after the subtraction of the Rayleigh scattering in the case without salt and SO_2 seeding. The strength of the Mie scattering signals is similar for the flows with only KCl or KOH seeding. The main difference between them is in the positions where aerosols are formed as shown in Fig. 5(c), which indicates different condensation temperatures for gaseous potassium species. The Mie scattering signal enhanced significantly as SO_2 was added through the McKenna burner flow as shown in Fig. 5(d) and (e). Meanwhile, no scattering was observed in the case with only SO_2 seeding (shown in Fig. 5(i)). The hot flue gas containing KOH produces a much stronger scattering signal with SO_2 than the hot flue gas containing KCl. The signal position also shifted down as SO_2 was added, which can be observed in Fig. 5(g).

The variation of the Mie scattering signal with the height in the center of the counter-flow (radial position = 0 mm) is shown in Fig. 6, together with the measured temperature distribution. For the cases with the lean flame, as the hot flue gas containing KCl was cooled by the N_2 flow without SO_2, aerosols were formed at the position where the temperature was between 700 and 1000 K (shown in Fig. 6(a)). These aerosols were identified as KCl, which has a vapor pressure of 0.2 mbar at 1000 K [12]. When SO_2 was induced in the N_2 flow, the scattering signal was enhanced significantly and shifted a bit to the hot flow side at a temperature between 1000 K and 1400 K. The aerosols formed at this temperature were considered to be condensed K_2SO_4, consistent with the fact that the vapor pressure of K_2SO_4, e.g., 0.04 mbar at 1300 K [12], is much lower than that of KCl [12], and thus K_2SO_4 can condense at a higher temperature. Gas-phase potassium sulfate was produced through the sulfation reactions between KCl and SO_2 and subsequently underwent homogeneous nucleation. As the seeding of SO_2 was increased by a factor of four, i.e., from 245 ppm to 980 ppm as shown in Fig. 6(a), the peak value of the signal increased almost by the same factor. This indicates that the amount of K_2SO_4 aerosols formed in the flow is controlled by the concentration of SO_2. This finding is in agreement with the results of Ekvall et al. [16] who varied the S/K ratio from 1 to 4.

As shown in Fig. 6(b), aerosols were also formed when KOH was seeded into the lean flame, but in a region with a temperature between 900 K and 1100 K. This phenomenon is surprising, considering that KOH has a considerably higher saturated vapor pressure than KCl at the

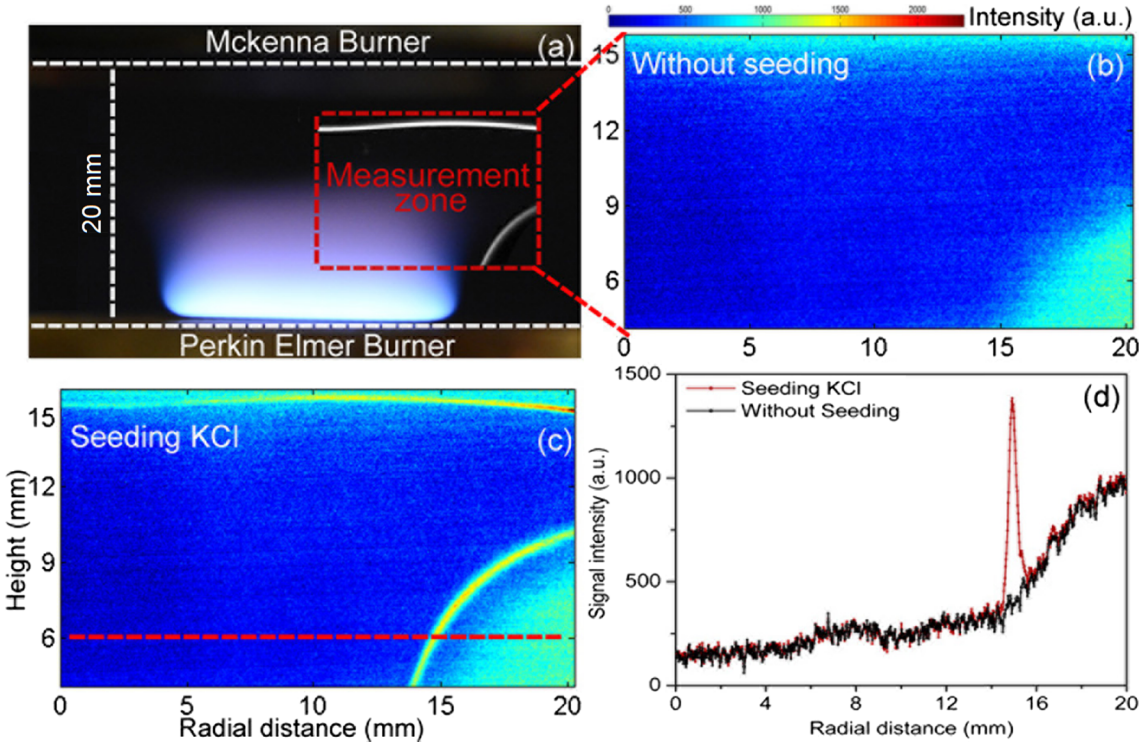

Fig. 3. The scattering signal measured in the counter-flow with the flame having equivalence ratio of 0.9. (a) Photo of the counter-flow with KCl seeding in the premixed flame. The box with red dash lines indicates the zone where the Rayleigh/Mie signal were captured; (b) The Rayleigh scattering signal of the counter-flow without seeding; (c) The scattering signal with KCl seeding; (d) The signal from (b) and (c) at height of 6 mm marked with the red dash line in (c). (For interpretation of the references to color in this figure legend, the reader is referred to the web version of this article.)

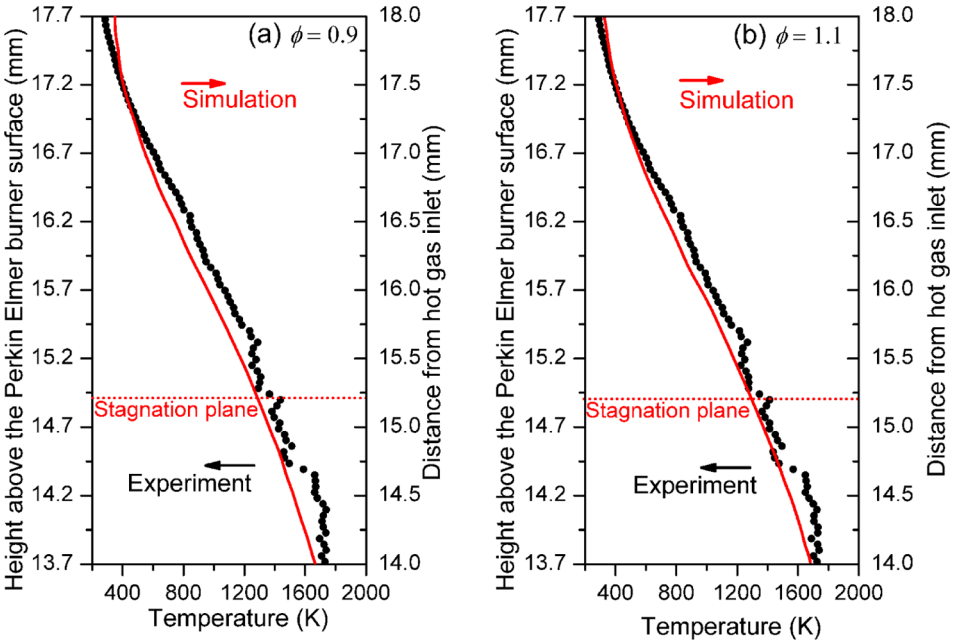

Fig. 4. The measured and predicted temperature profiles of the counter-flow from the fuel-lean (a) and the fuel-rich (b) flame. The location of the stagnation plane for the two flames was indicated with dash lines.

same temperature (e.g. 8 mbar for KOH at 1100 K vs. 1.5 mbar for KCl at 1100 K [24]). Conceivably the aerosols consist of potassium carbonate (K_2CO_3), which, according to equilibrium calculations with FactSage 7.0, is stable in condensed form under these conditions (see Supplementary Material). This might happen as the reverse process of the decomposition of K_2CO_3 [25], i.e., $2KOH + CO_2 = K_2CO_3 + H_2O$ (R13), $K_2CO_3 = K_2CO_3(s)$ (R14). This sequence is promoted by the presence of ~8% CO_2 in the flue gas. Formation of potassium carbonate in the gas-phase is not favored thermodynamically, but conceivably a small amount of gaseous K_2CO_3 can be formed and nucleate homogeneously [26].

Similar to the flame with KCl seeding, K_2SO_4 aerosols were detected as KOH mixed with the SO_2 from the N_2 flow. However, the intensity of the scattering signal was much stronger than for KCl seeding, indicating

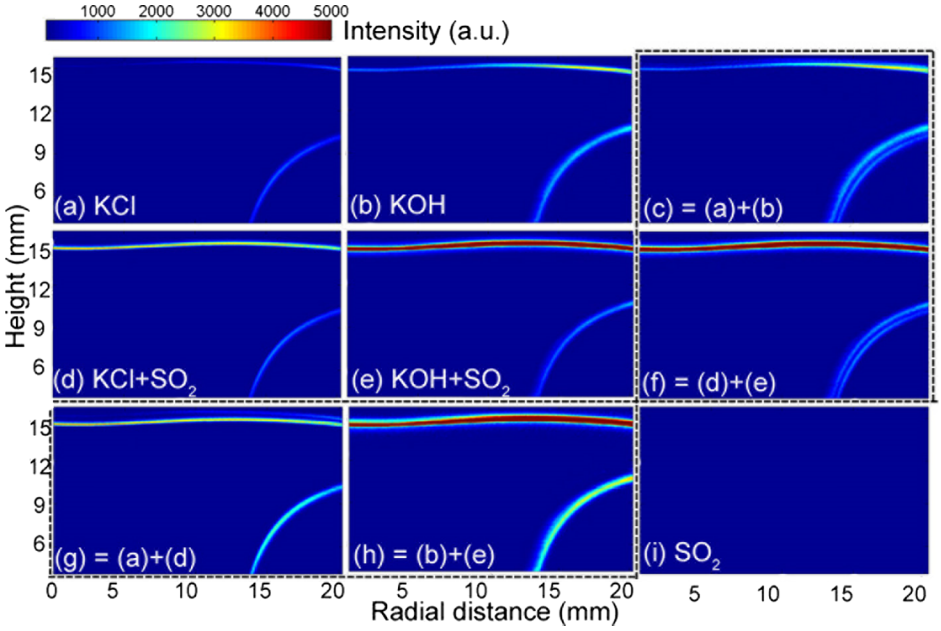

Fig. 5. The Mie scattering signal from aerosols generated in the counter-flow ($\phi = 0.9$) under different seeding conditions. (a) with seeding of KCl solution; (b) with seeding of KOH solution; (c) combination of the results in (a) and (b); (d) with seeding of KCl solution and with SO_2 in the N_2 flow from the McKenna burner; (e) with seeding of KOH and with SO_2; (f) combination of the results in (d) and (e); (g) combination of the results in (a) and (d); (h) combination of the results in (b) and (e); (i) only with SO_2 in the N_2 flow. Note: The signal over 5000 counts is saturated in the chosen color bar in order to visualize the weak scattering. The accurate intensity reading is to be found in Fig. 6.

that aerosols were formed in larger amounts during sulfation of KOH. Hence, gas-phase sulfation of KOH by SO_2 appears to occur more readily than homogeneous sulfation of KCl. Moreover, as the concentration of SO_2 was increased from 245 ppm to 980 ppm, the peak of the scattering signal in the KOH case in Fig. 6(b) only doubled, indicating that the sulfation reaction was no longer first order in SO_2.

Results for the fuel-rich flames ($\phi = 1.1$) are shown in Fig. 6(c) and (d). Again, the Mie scattering signal was detected as SO_2 was seeded into the flow, but the signal was weaker by more than a factor of 10 comparing to the corresponding lean flame ($\phi = 0.9$). The reduction in the signal is attributed to the lack of oxidizer (O_2) under the fuel-rich conditions, since oxidation is required in the sulfation process between KCl/KOH and SO_2. Moreover, the signal intensity became almost independent of the concentration of SO_2. Besides, under the condition of KCl seeding, the aerosol signals are detected at relatively low temperatures (between 800 K and 1000 K) and it is uncertain whether the aerosols consist of K_2SO_4. An assumption can be that the K_2SO_4 is also formed under this condition, but its lower concentration induces a lower nucleation temperature based on the relationship between its saturated vapor pressure and temperature.

The reaction between KCl (215 ppm)/KOH (215 ppm) and SO_2 (245 ppm and 980 ppm) in counter-flow was modeled with the detailed reaction mechanism. The results for the KCl and KOH flames, respectively, seeded with 245 ppm SO_2 and for equivalence ratios of 0.9 and 1.1 are presented in Fig. 7. The figure shows the region 14–18 mm from the hot gas inlet, where K_2SO_4 was formed as KCl/KOH was sulfated by SO_2 during the mixing between the hot flue gas and the cold N_2/SO_2 flow. In this region the predicted temperature and its variation with position agree well with the experiments (see Fig. 4). The predicted concentration profiles of K_2SO_4 under different conditions in Fig. 7 are consistent with the measurements. The model predicts that K_2SO_4 has its concentration peak at a temperature around 1200 K, where the condensation of K_2SO_4 happens and aerosols are formed according to its saturated vapor pressure [12]. In agreement with observations, the

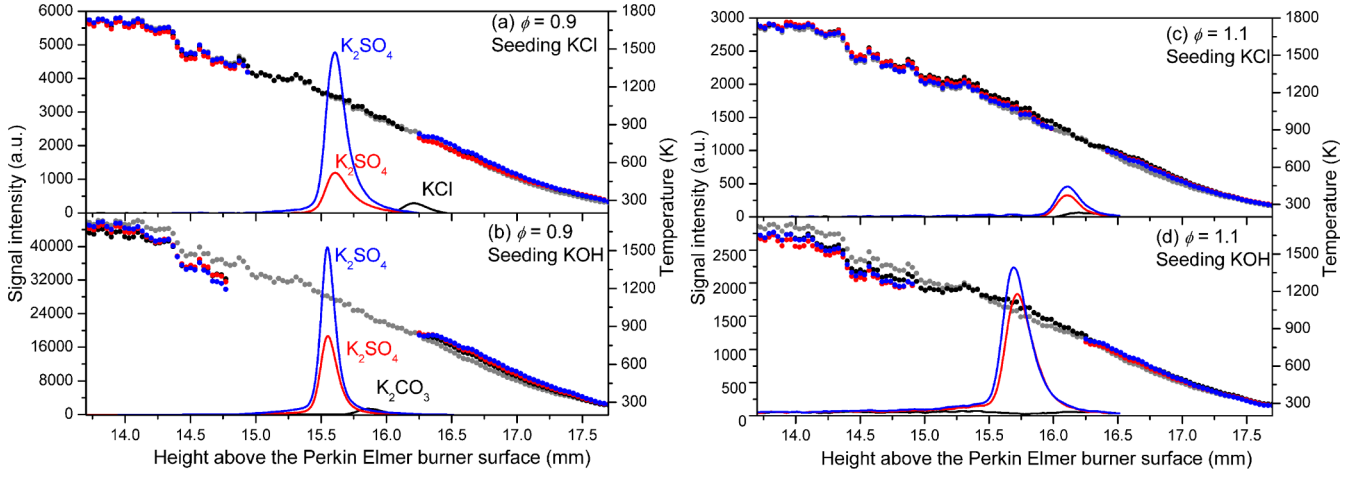

Fig. 6. The vertical distribution of the measured temperature and the Mie scattering from aerosols along the center of the counter flow at different conditions. (a) Seeding of KCl into the flame at equivalence ratio of 0.9; (b) Seeding of KOH into the flame at equivalence ratio of 0.9; (c) Seeding of KCl into the flame at equivalence ratio of 1.1; (d) Seeding of KOH into the flame at equivalence ratio of 1.1. Dot lines indicate temperature distribution; solid lines indicate the Mie scattering signal; different color indicates different seeding conditions: without seeding salt solution (gray); seeding salt solution without SO_2 (black); seeding salt solution with 245 ppm SO_2 (red); seeding salt solution with 980 ppm SO_2 (blue). (For interpretation of the references to color in this figure legend, the reader is referred to the web version of this article.)

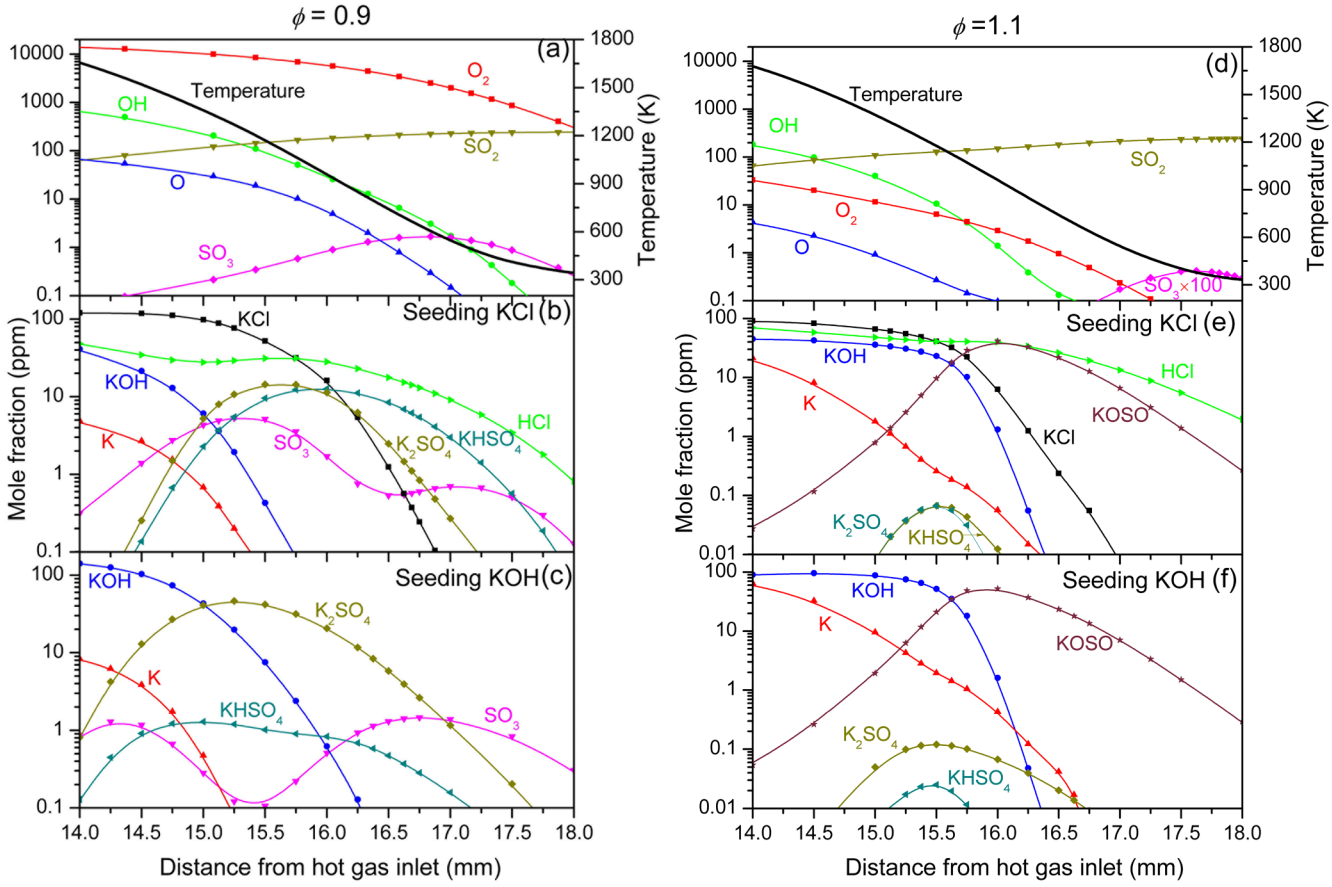

Fig. 7. The simulated mole fraction distributions of key species and temperature along the center of the counter flow reactor of different conditions at equivalence ratio of 0.9 and 1.1. The seeding condition: 245 ppm SO_2 without salt seeding (a, d), with 215 ppm KCl (b, e) and 215 ppm KOH (c, f).

model predicts KOH to be sulfated more readily than KCl, yielding larger concentrations of K_2SO_4 in the KOH doped flame. As expected, much less K_2SO_4 was predicted in the rich flame case with insufficient O_2.

Fig. 8 shows reaction path diagrams for the reaction conditions of Fig. 7. Even though the modeling predictions are consistent with the experimental observations, the path analysis must be interpreted with caution since many of the key reactions in the model have not been confirmed experimentally. According to the model, the sulfation pathways involving SO_3, i.e., $KCl + SO_3(+M) = KSO_3Cl(+M)$ (R1), $KSO_3Cl + H_2O = KHSO_4 + HCl$ (R3), $KHSO_4 + KCl = K_2SO_4 + HCl$ (R4) for KCl doping and $KOH + SO_3(+M) = KHSO_4(+M)$ (R2), $KHSO_4 + KOH = K_2SO_4 + H_2O$ (R5) for KOH doping, are only of minor importance for formation of K_2SO_4 under the investigated conditions. The SO_3 pathway is most important in sulfation of KCl in the low temperature region (< 1000 K) of the lean flame, where a small amount of SO_3 (~1 ppm) is generated in the mixing region (Fig. 7(a)).

For both KCl and KOH, the major sulfation pathway is predicted to involve atomic potassium, formed in significant amounts from thermal dissociation of KCl and KOH, respectively (Fig. 7(b) and (c)). The concentration of atomic K can be 1 ppm with 10 ppm of KOH at the temperature of ~1500 K.

The K-atom is then converted to $KOSO_3$, either through $K + SO_2 (+M) = KOSO (+M)$ (R15), $KOSO + O_2 (+M) = KOSO_3 (+M)$ (R16) or via $K + O_2 (+M) = KO_2 (+M)$ (R10), $KO_2 + SO_2 (+M) = KOSO_3(+M)$ (R11). These reactions are promoted by the availability of O_2 and of SO_2, which diffuses from the cool N_2 side with a concentration of ~100 ppm.

Once formed, $KOSO_3$ may react with KOH to form K_2SO_4 directly, $KOSO_3 + KOH = K_2SO_4 + OH$ (R17), or through the sequence $KOSO_3 + H_2O = KHSO_4 + OH$ (R12), $KHSO_4 + KOH = K_2SO_4 + H_2O$ (R5).

An analysis of the A-factor sensitivity of the predicted K_2SO_4 concentration shows that the sulfation rate is always sensitive to the reactions $KO_2 + SO_2 (+M) = KOSO_3(+M)$ (R11) and $K + SO_2 (+M) = KOSO (+M)$ (R15), except at low temperature (~900 K at ~16 mm) for KCl sulfation where it becomes sensitive to $KCl + SO_3(+M) = KSO_3Cl(+M)$ (R1). The rate constant for reaction R15 was measured at 863 K by Goumri et al. [27], while the value of k_{11} is a rough estimate from Hindiyarti et al. [11]. Both rate constants can be expected to be complex functions of temperature and pressure and involve considerable uncertainties.

Comparing the sulfation of KOH and KCl, less K_2SO_4 was formed from KCl. This can be explained from the analysis of the calculations. As shown in Fig. 7(b) and (c), atomic K was formed in lower concentrations from KCl compared KOH. Thermal dissociation of KCl and KOH does not show up in the sensitivity analysis since both steps are rapidly equilibrated. However, KOH is thermodynamically less stable than KCl, leading to larger levels of atomic K.

The sulfation processes in the rich flames are similar to those occurring in the lean flames, according to our simulations. However, even though sufficient K_2SO_4 was produced to form aerosols at a temperature around 1100 K, the concentration of K_2SO_4 is much lower in the rich flames, in agreement with the experimental results. The difference is attributed to the low concentration of oxidants, which is two orders of magnitude smaller than for the lean cases. Thus, the amount of SO_3 formed in the rich flames becomes negligible, especially in the region where most K_2SO_4 was formed (at ~15.5 mm). Any SO_3 formed can be consumed rapidly by H atoms. There is almost no contribution from R1, R2 and R3 to the sulfation. The sulfation process was dominated by the

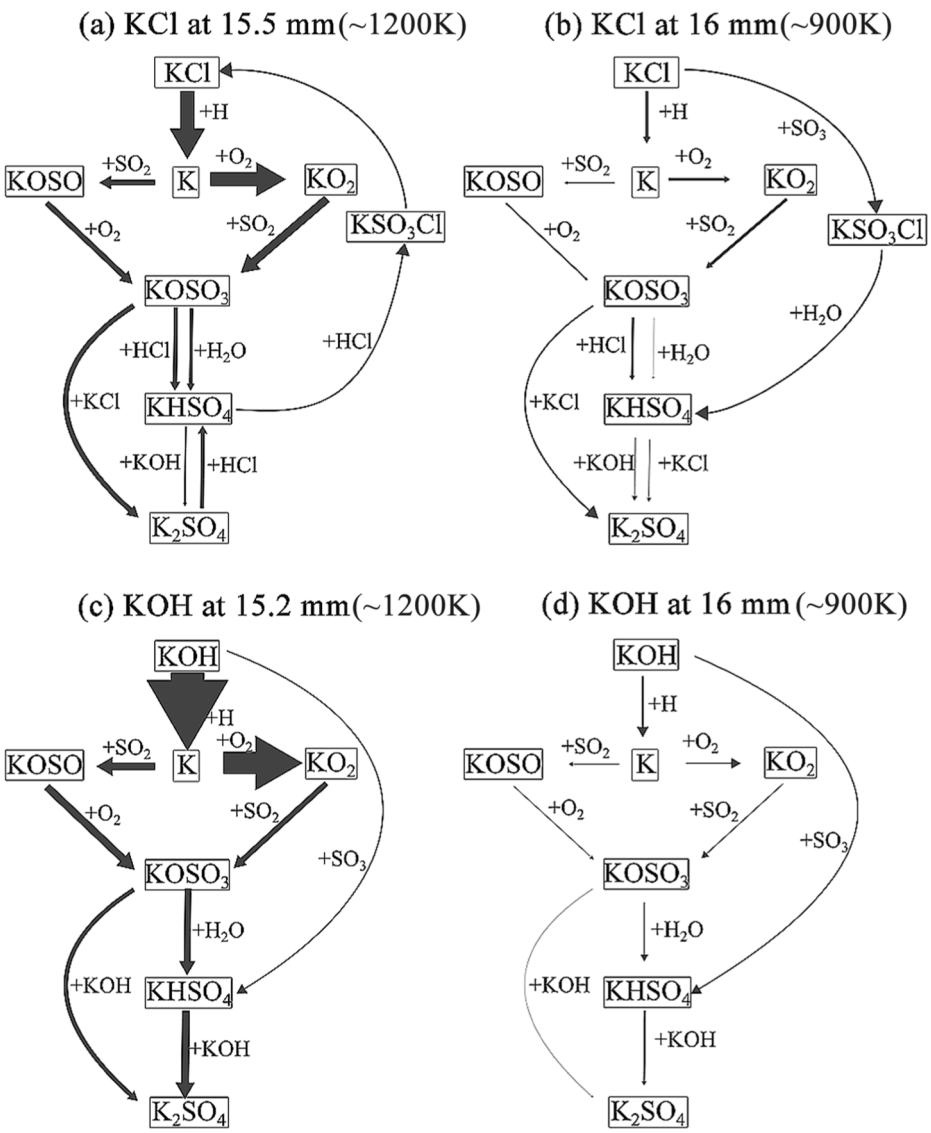

Fig. 8. Reaction pathways for the formation of K_2SO_4 from KCl (215 ppm) and KOH (215 ppm) with SO_2 (245 ppm) at the position having the K_2SO_4 concentration peak (~1200 K) (a, c) and a low temperature (~900 K) (b, d). For KCl, the K_2SO_4 concentration peak is at 15.5 mm; For KOH, it is 15.2 mm; the position at 16 mm is selected as the low temperature region. The line thickness indicates the relative strength of the reactions. The flame with equivalence ratio of 0.9 is used to provide the hot gas.

pathway through $KOSO_3$ as discussed for the lean conditions. In the rich flames, a high concentration of K atom was predicted in the hot gas (e.g. more than 10 ppm K atom is predicted in the hot gas at ~1500 K with KOH seeding). However, due to the lack of oxidants, reaction R16, i.e. the oxidation of KOSO by O_2, becomes the rate-limiting step. KOSO is generated easily through R15 and becomes a major potassium compound, especially in the low temperature region with sufficient SO_2 (see Fig. 7(e) and (f)).

In the simulation, as the seeding of SO_2 increased from 245 ppm to 980 ppm with the KCl/KOH seeding remaining at 215 ppm, the increment ratio of the K_2SO_4 concentration is always much smaller than the increment ratio of the SO_2 seeding. This can also be observed in most measurement results, but the sulfation of KCl in the lean flame is an exception, in which the strength of the scattering signal almost had the same increment ratio as the concentration of SO_2. The simulations might underestimate the importance of the sulfation pathway through R1 and R3 for KCl at low temperature region (< 1000 K) where the formation and condensation of K_2SO_4 can happen at the same time. If the effect of the condensation of K_2SO_4 was taken into consideration in the modeling, more aerosols would be formed through this sulfation pathway.

4. Conclusions

In the present work, sulfation of KCl and KOH by SO_2 in hot flue gases was investigated. Simultaneous measurement of the temperature distribution and detection of aerosol formation in a counter-flow system allowed identification of aerosols as consisting of KCl K_2SO_4, and K_2CO_3, respectively, depending on the potassium speciation in the inlet and the availability of SO_2. The experiments showed that KOH was sulphated more readily than KCl, resulting in larger quantities of aerosols. The sulfation process in the counter-flow setup was simulated using a chemical kinetic model including a detailed subset for the Cl/S/K chemistry. Similar to the experimental results, much more potassium sulfate was predicted when seeding KOH compared to seeding KCl. For both KOH and KCl, sulfation was predicted to occur primarily through the reactions among atomic K, O_2 and SO_2, forming $KHSO_4$ and K_2SO_4. The higher propensity for sulfation of KOH compared to KCl was mostly attributed to the lower thermal stability of KOH, facilitating formation of atomic K. According to the model, some sulfation also happened

through SO_3 in the low temperature region (< 1000 K), especially for KCl ($KCl \rightarrow KSO_3Cl \rightarrow K_2SO_4$). To obtain a better understanding of the sulfation process for different Cl/K and S/K ratios, more quantitative measurements on the concentrations of KOH, KCl, K atom, and SO_2 in the reaction region are needed. The authors' group has recently obtained spectral-resolved quantitative UV absorption cross section of KCl and KOH [28], which will be used for in situ KCl, KOH and SO_2 concentration measurement in a novel multi-jet burner [29] to generate quantitative data for accurate kinetic understanding of the sulfation processes.

Acknowledgements

The work was financially supported by the Swedish Energy Agency, the Knut & Alice Wallenberg foundation, the Swedish Research Council (VR), the European Research Council (Advanced Grant TUCLA program) and the Danish Council for Strategic Research (the GREEN project).

Appendix A. Supplementary data

Supplementary data associated with this article can be found, in the online version, at https://doi.org/10.1016/j.fuel.2018.03.095.

References

[1] Sims REH, Hastings A, Schlamadinger B, Taylor G, Smith P. Energy crops: current status and future prospects. Global Change Biol 2006;12(11):2054–76.
[2] Werther J, Saenger M, Hartge EU, Ogada T, Siagi Z. Combustion of agricultural residues. Prog Energy Combust Sci 2000;26(1):1–27.
[3] Sun Y, Liu L, Wang Q, Yang X, Tu X. Pyrolysis products from industrial waste biomass based on a neural network model. J Anal Appl Pyrolysis 2016;120:94–102.
[4] Schofield K. The chemical nature of combustion deposition and corrosion: the case of alkali chlorides. Combust Flame 2012;159(5):1987–96.
[5] Aho M, Vainikka P, Taipale R, Yrjas P. Effective new chemicals to prevent corrosion due to chlorine in power plant superheaters. Fuel 2008;87(6):647–54.
[6] Wu H, Pedersen MN, Jespersen JB, Aho M, Roppo J, Frandsen FJ, et al. Modeling the use of sulfate additives for potassium chloride destruction in biomass combustion. Energy Fuels 2014;28(1):199–207.
[7] Kassman H, Bäfver L, Åmand L-E. The importance of SO_2 and SO_3 for sulphation of gaseous KCl – an experimental investigation in a biomass fired CFB boiler. Combust Flame 2010;157(9):1649–57.
[8] Iisa K, Lu Y, Salmenoja K. Sulfation of potassium chloride at combustion conditions. Energy Fuels 1999;13(6):1184–90.
[9] Jiménez S, Ballester J. Influence of operating conditions and the role of sulfur in the formation of aerosols from biomass combustion. Combust Flame 2005;140(4):346–58.
[10] Glarborg P, Marshall P. Mechanism and modeling of the formation of gaseous alkali sulfates. Combust Flame 2005;141(1–2):22–39.
[11] Hindiyarti L, Frandsen F, Livbjerg H, Glarborg P, Marshall P. An exploratory study of alkali sulfate aerosol formation during biomass combustion. Fuel 2008;87(8–9):1591–600.
[12] Garba MU, Ingham DB, Ma L, Porter RTJ, Pourkashnian M, Tan HZ, et al. Prediction of potassium chloride sulfation and its effect on deposition in biomass-fired boilers. Energy Fuels 2012;26(11):6501–8.
[13] Kassman H, Normann F, Åmand L-E. The effect of oxygen and volatile combustibles on the sulphation of gaseous KCl. Combust Flame 2013;160(10):2231–41.
[14] Li B, Sun Z, Li Z, Aldén M, Jakobsen JG, Hansen S, et al. Post-flame gas-phase sulfation of potassium chloride. Combust Flame 2013;160(5):959–69.
[15] Ekvall T, Normann F, Andersson K, Johnsson F. Modeling the alkali sulfation chemistry of biomass and coal co-firing in oxy-fuel atmospheres. Energy Fuels 2014;28(5):3486–94.
[16] Ekvall T, Andersson K, Leffler T, Berg M. K–Cl–S chemistry in air and oxy-combustion atmospheres. Proc Combust Inst 2017;36(3):4011–8.
[17] Hsu L-J, Alwahabi ZT, Nathan GJ, Li Y, Li ZS, Aldén M. Sodium and potassium released from burning particles of brown coal and pine wood in a laminar premixed methane flame using quantitative laser-induced breakdown spectroscopy. Appl Spectrosc 2011;65(6):684–91.
[18] Li B, Li Y, Wang Z, Li Z, Sun Z, Aldén M. A novel multi-jet quartz burner for laminar near-adiabatic flames: Standards of temperatures calibration of laser diagnostics techniques. In: 4th European combustion meeting. Vienna, Austria; 2009.
[19] CHEMKIN 10131, Reaction Design: San Diego, 2013.
[20] Hashemi H, Christensen JM, Gersen S, Glarborg P. Hydrogen oxidation at high pressure and intermediate temperatures: experiments and kinetic modeling. Proc Combust Inst 2015;35(1):553–60.
[21] Song Y, Hashemi H, Christensen JM, Zou C, Haynes BS, Marshall P, et al. An exploratory flow reactor study of H_2S oxidation at 30–100 bar. Int J Chem Kinet 2017;49(1):37–52.
[22] Pelucchi M, Frassoldati A, Faravelli T, Ruscic B, Glarborg P. High-temperature chemistry of HCl and Cl2. Combust Flame 2015;162(6):2693–704.
[23] Sorvajärvi T, Viljanen J, Toivonen J, Marshall P, Glarborg P. Rate Constant and Thermochemistry for $K + O_2 + N_2 = KO_2 + N_2$. J Phys Chem A 2015;119(14):3329–36.
[24] Available from: http://webbook.nist.gov/.
[25] Lehman RL, Gentry JS, Glumac NG. Thermal stability of potassium carbonate near its melting point. Thermochim Acta 1998;316(1):1–9.
[26] Hildenbrand D, Lau K. Mass spectrometric searches for gaseous sodium carbonates. J Phys Chem 1991;95(22):8972–5.
[27] Goumri A, Laakso D, Rocha JDR, Francis E, Marshall P. Investigation of the gas-phase kinetics of the reaction potassium + sulfur dioxide + argon. J Phys Chem 1993;97(20):5295–7.
[28] Weng W, Leffler T, Brackmann C, Aldén M, Li Z. Spectrally resolved UV absorption cross-sections of alkali hydroxides and chlorides measured in hot flue gases. accepted by Appl Spectrosc.
[29] Weng W, Borggren J, Li B, Aldén M, Li Z. A novel multi-jet burner for hot flue gases of wide range of temperatures and compositions for optical diagnostics of solid fuels gasification/combustion. Rev Sci Instrum 2017;88(4):045104.